

Supplement of  
**Long-range transported pollution from the Middle East and its  
impact on carbonaceous aerosol sources over Cyprus.**

5 Christodoulou A. et al

*Correspondence to:* Alikı Christodoulou ([a.christodoulou@cyi.ac.cy](mailto:a.christodoulou@cyi.ac.cy)) and Jean Sciare ([j.sciare@cyi.ac.cy](mailto:j.sciare@cyi.ac.cy))

Section S1. PMF methodology

Initially, the reference factor profile (RFP) BBOA from Ng et al., 2011 was used to constrain the PMF. The m/z 60 cannot be explained by any combination of a-values (constrained). The combinations presented in Table S1 have been used and resulted in non-optimum correlations between BC<sub>wb</sub> vs BBOA. The correlation of BC<sub>wb</sub> with the other factor that contained m/z 60 was better with an R<sup>2</sup> up to 0.84.

**Table S1: Changes in correlation coefficient of BC<sub>ff</sub> vs HOA-1 and BC<sub>wb</sub> and BC<sub>wb</sub> vs BBOA for different a-values used to constrained the BBOA mass spectrum.**

a-value	r <sup>2</sup> of BC <sub>ff</sub> vs HOA-1	r <sup>2</sup> of BC <sub>wb</sub> vs BBOA
0.3	0.53	0.66
0.35	0.54	0.26
0.4	0.56	0.01
0.45	0.56	0.02

The second step was to search for a local BBOA factor. The unconstrained solutions have shown very good correlation for BBOA vs BC<sub>wb</sub>. Thus, the unconstrained runs have been used to calculate the local BBOA reference factor. Both 4-factor and 5-factor solution runs were tested. For the 4-factor solution, the HOA factor retrieved had a clear pattern containing the alkane and alkene related fragments and wasn't containing m/z 44. BBOA factor retrieved was containing 99% of the m/z 60 included in the dataset. The 5-factor solution of unconstrained PMF runs exhibits a separation between primary and secondary factors, however the solution among the runs isn't that stable. Critically, the BBOA profile factor wasn't as stable as in the 4-factor solution (Fig. S1).

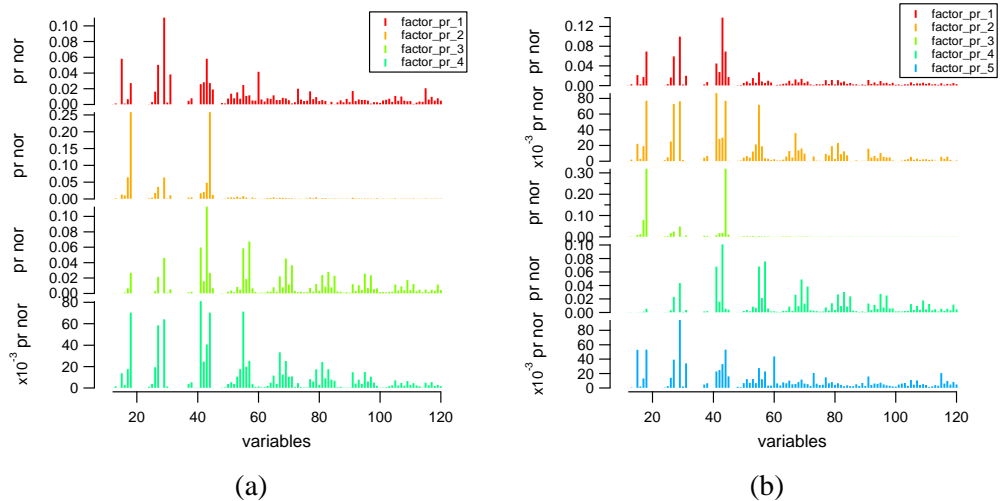


**Figure S1. Factor profiles for the four- (a) and five- (b) factor unconstrained runs for the 2017 cold period dataset.**

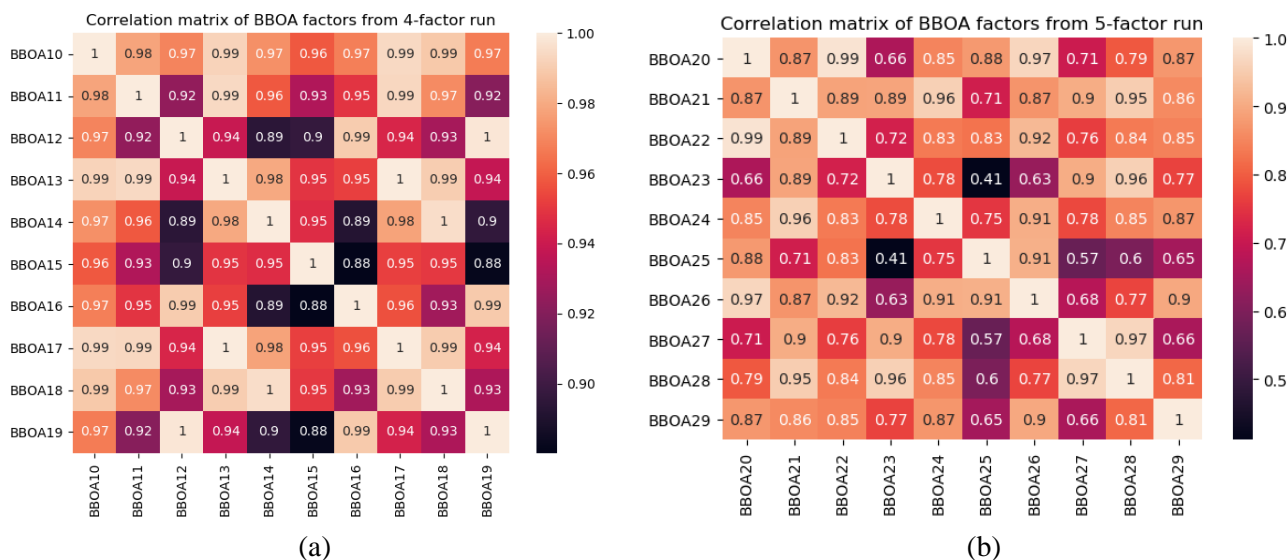


**Figure S2. Coefficient of determination for linear regression ( $r^2$ ) of deconvolved BBOA profiles from the 4-factor unconstrained run (a) and 5-factor unconstrained run (b).**

As observed in Fig. S2, the 4-factor solution was having quite similar factor profiles for BBOA compared to the 5-factor unconstrained runs. Thus, the 4-factor solution has been used to derive this BBOA-like local factor in Nicosia (BBOA<sub>cy</sub> more effectively. In the figure S3 the mass spectra of the calculated BBOA<sub>cy</sub> is presented.

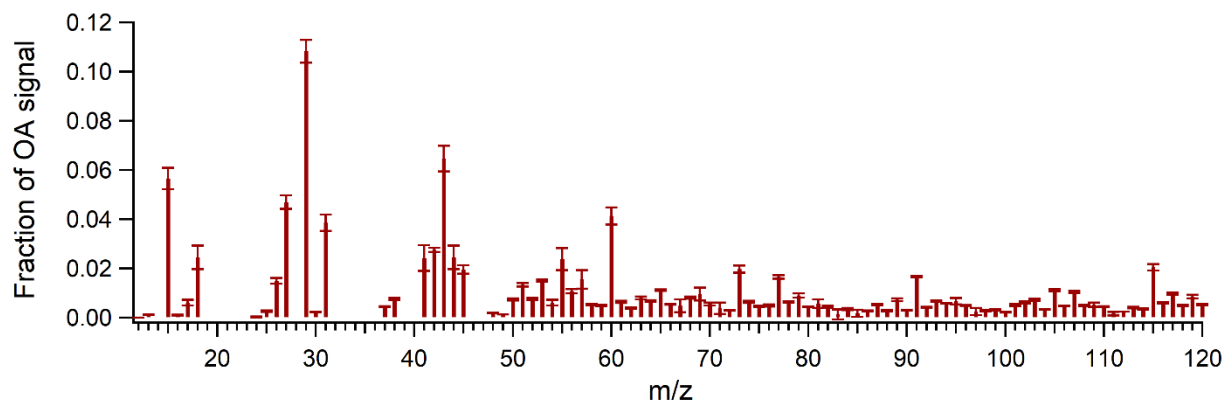


**Figure S3: The mass spectra of the calculated BBOA<sub>cy</sub> averaging the unconstrained solutions. Error bars represent one standard deviation of the averaged unconstrained solutions.**

Applying  $a$ -values (0-0.5 with a step of 0.02) for the BBOA<sub>cy</sub> revealed that the best solution was to use an  $a$ -value of 0.46. It was the most stable solution among all, having good correlation of BBOA factor with BC<sub>wb</sub> ( $r^2 = 0.84$ ), and HOA factor with BC<sub>ff</sub> ( $r^2 = 0.67$ ). Additionally, the  $a$ -value of 0.46 also had the most stable factor profile results.

Afterwards, the optimum a-value for HOA was selected. To do so, the BBOA<sub>cy</sub> factor was anchored with an a-value of 0.46 and a first-dimension sensitivity analysis for the HOA-like reference factor from Ng et al., (2011) was used with a-values ranging from 0 to 0.2 with a step of 0.02. All a-values ranging 0.1 to 0.2 resulted in similar correlation between HOA factors and BC<sub>ff</sub> ( $r^2 = 0.65$ ). However, the contribution of HOA factor increased as the a-value was increased. Finally, the a-value of 0.2 was selected so that maximum freedom was given to the system to explain all possible emissions from fossil fuel combustion.

## Section S2. Supplementary Figures

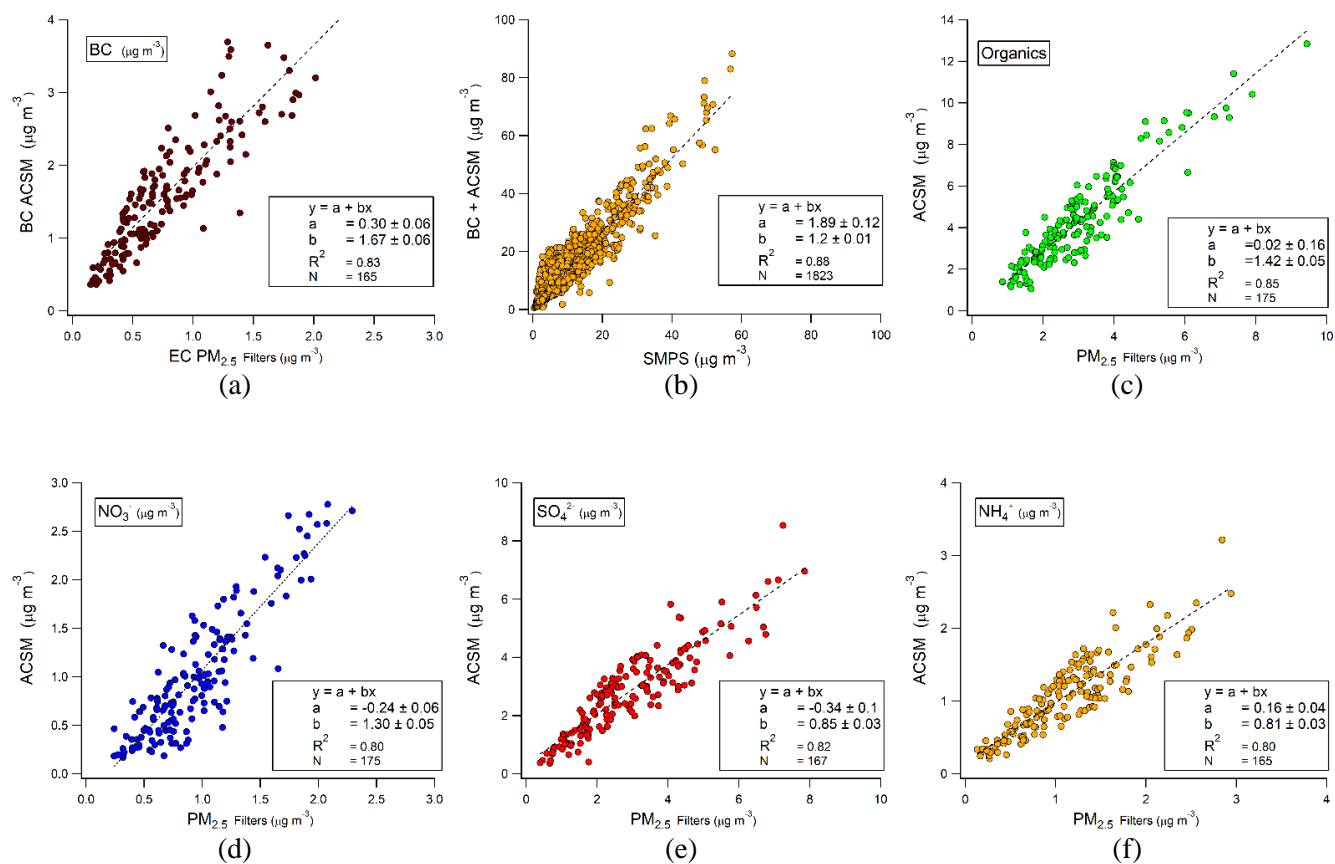
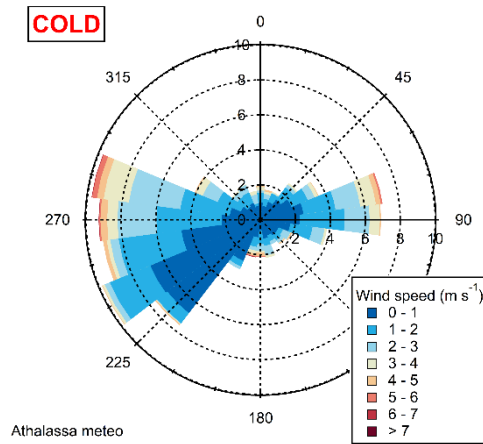
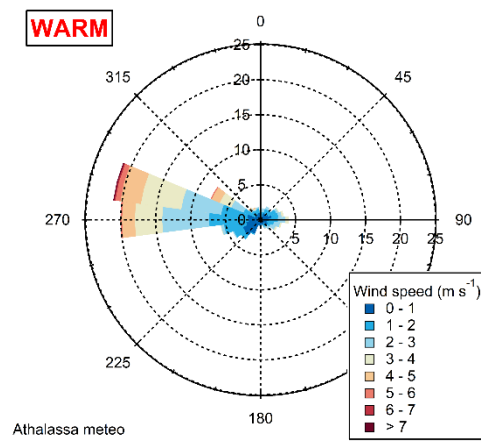


Figure S4: a) Comparison of daily average BC and EC concentrations b) Mass closure exercise between daily averaged reconstructed PM<sub>1</sub> (ACSM+BC) and measured PM<sub>1</sub> by SMPS. c-f) Scatterplot of chemically speciated ACSM measurements versus filter analyses for organic matter (compared to OC filter- based measurements), nitrate, sulfate and ammonium.

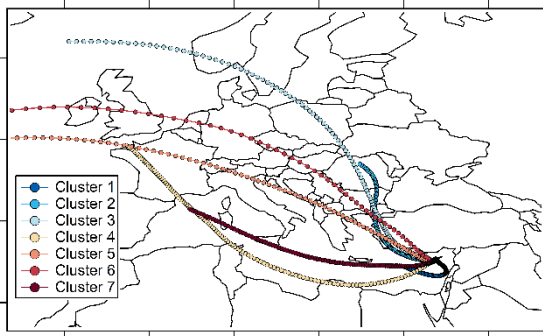


(a)

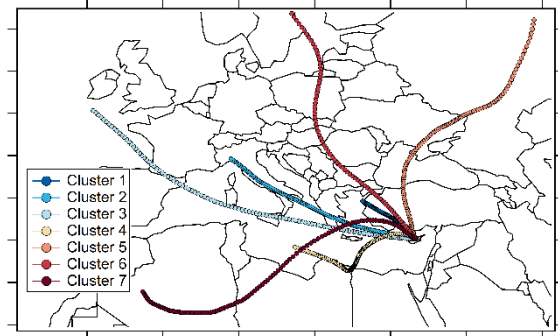


(b)

Figure S5. Wind roses for (a) the cold season and (b) the warm season respectively. Wind direction and velocity data obtained by the Athassa Forestry Park Meteorological Station operated by the Cyprus Department of Meteorology.

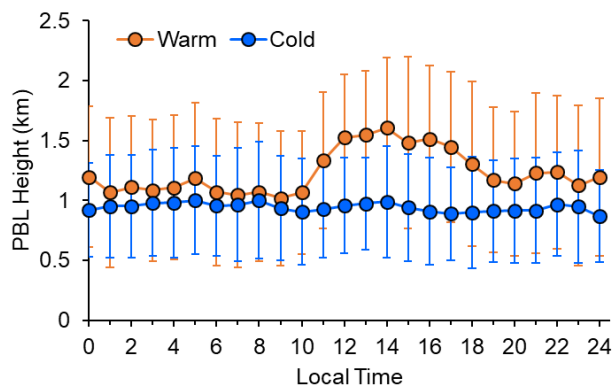


(a)



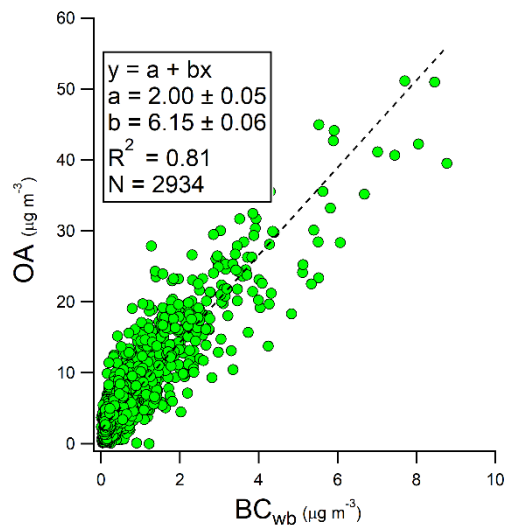
(b)

Figure S6: Cluster analysis for backward trajectories of air masses during the cold (a) and warm (b) period.

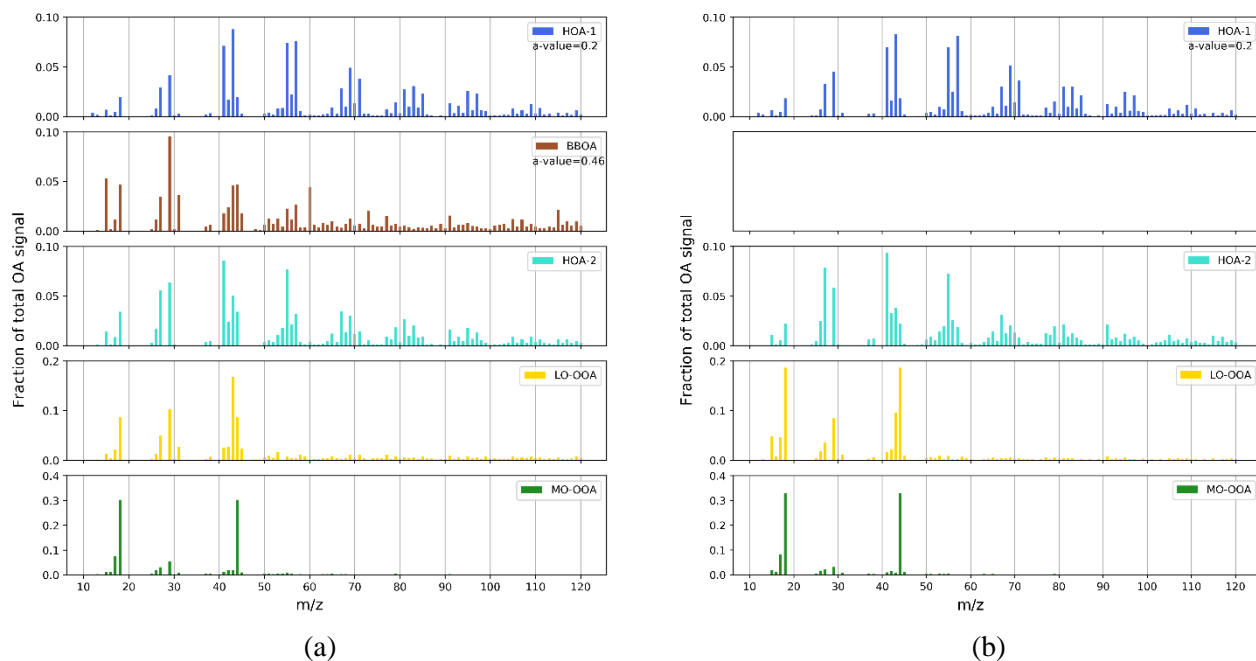


**Figure S7: Diurnal profile of the planetary boundary layer height calculated by the LIDAR measurements for both periods in Nicosia**

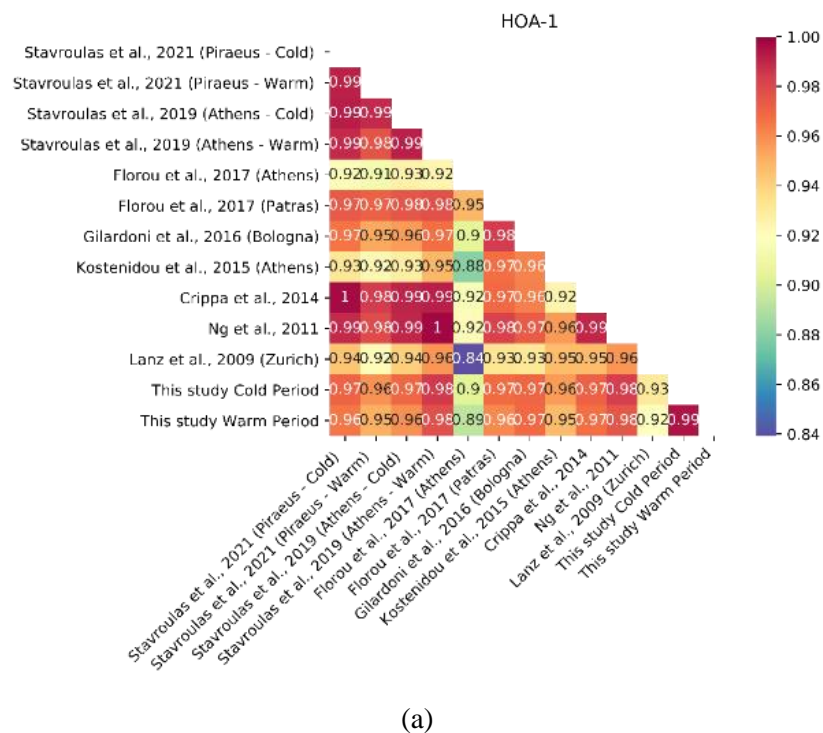
60



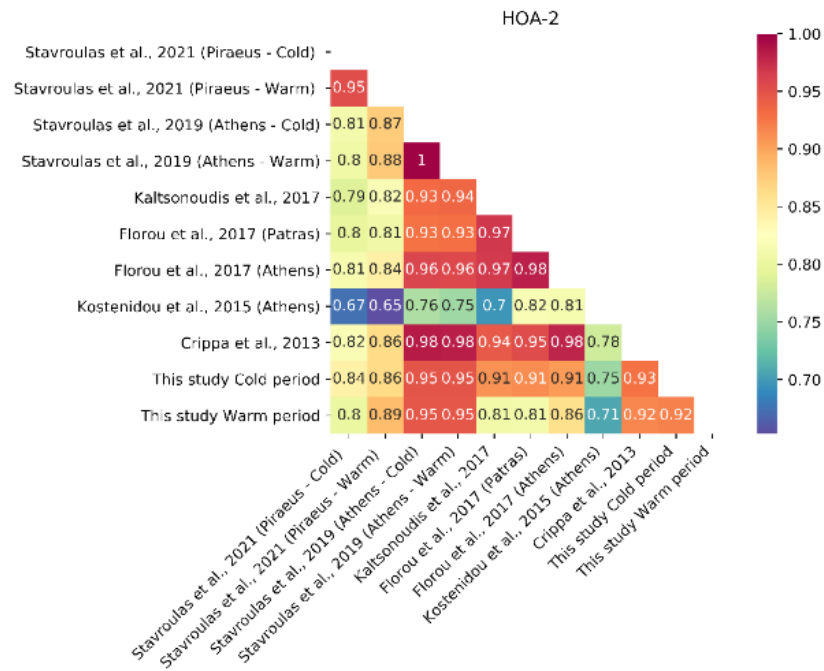
**Figure S8: Scatter plot and linear regression of OA measured in Nicosia during the cold period versus  $BC_{wb}$  obtained by the aethalometer model**



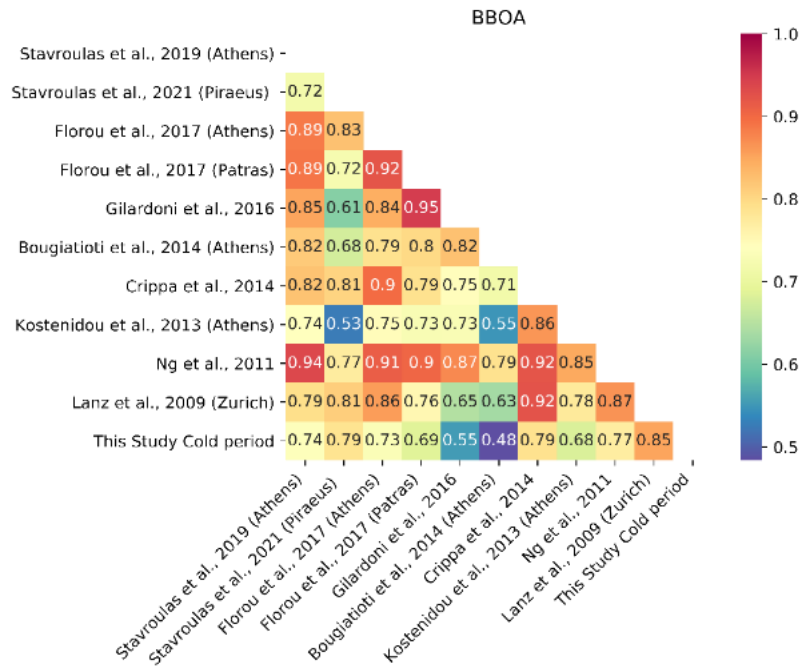
65 **Figure S9: Mass spectra of the PMF derived OA factors for (a) the cold and (b) the warm period under study in Nicosia.**



(a)

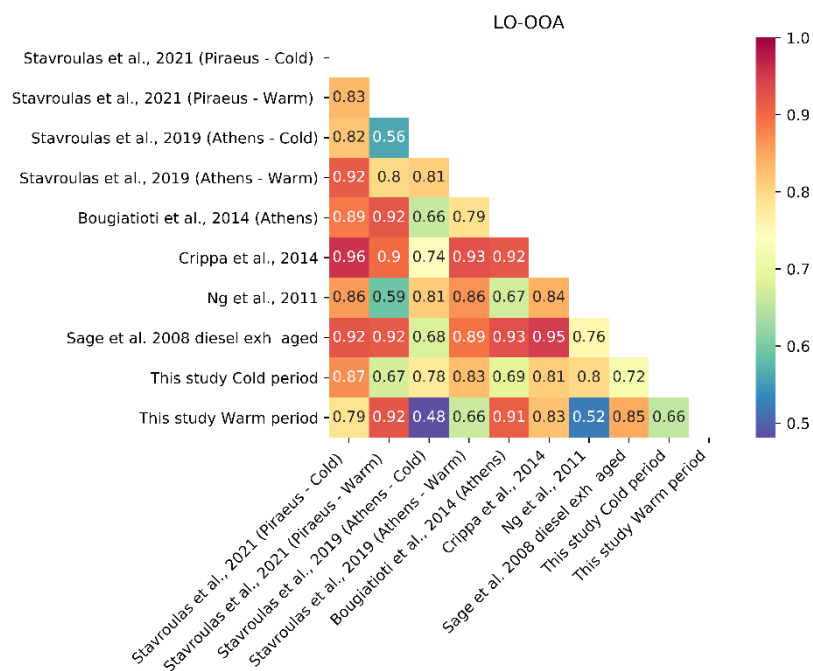


(b)

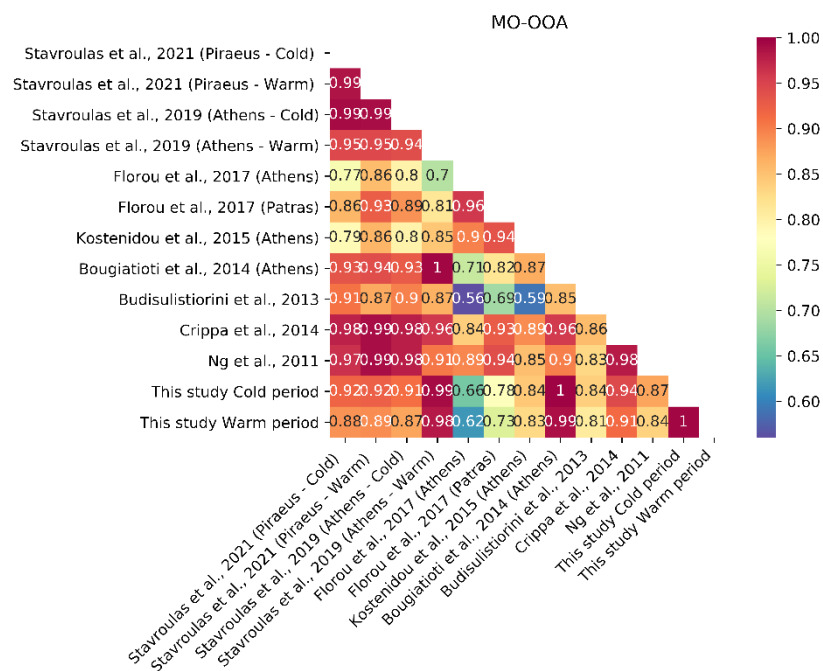


(c)



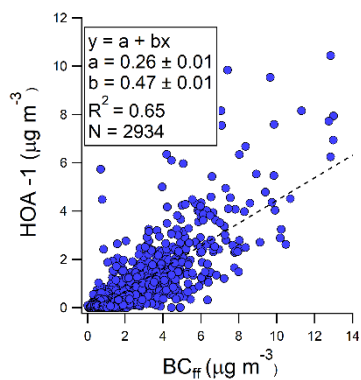


(d)

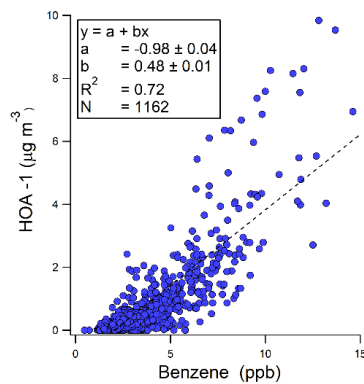


(e)

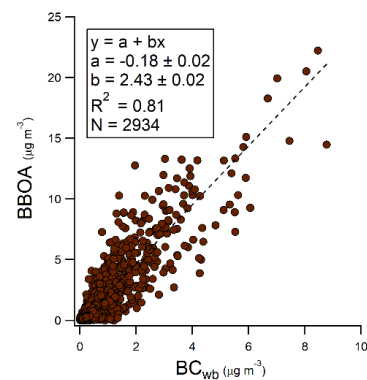
**Figure S10: Correlation matrices of resolved OA factor profiles against selected factor profiles found in the literature.**



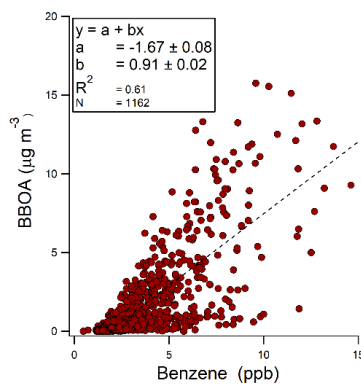
(a)



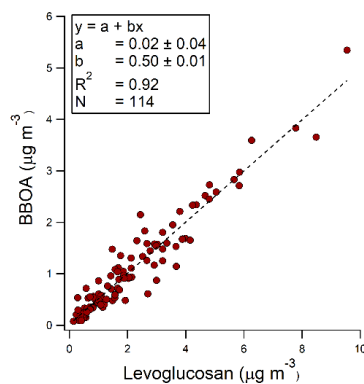
(b)



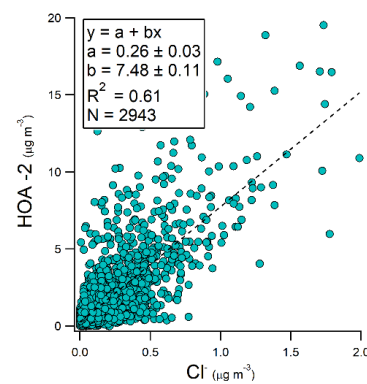
(c)



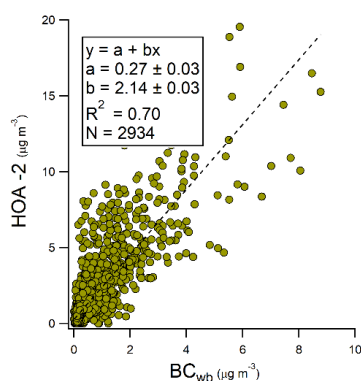
(d)



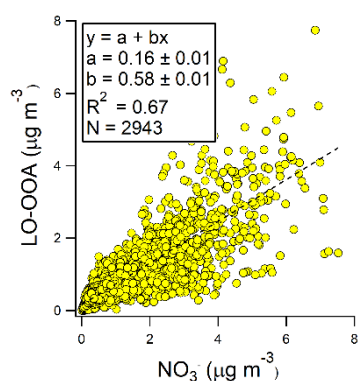
(e)



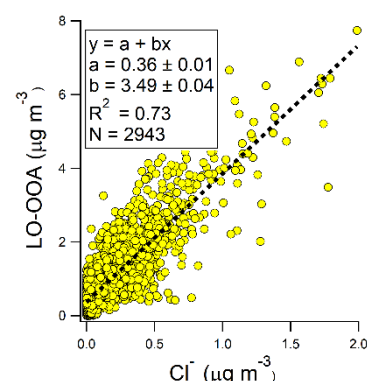
(f)



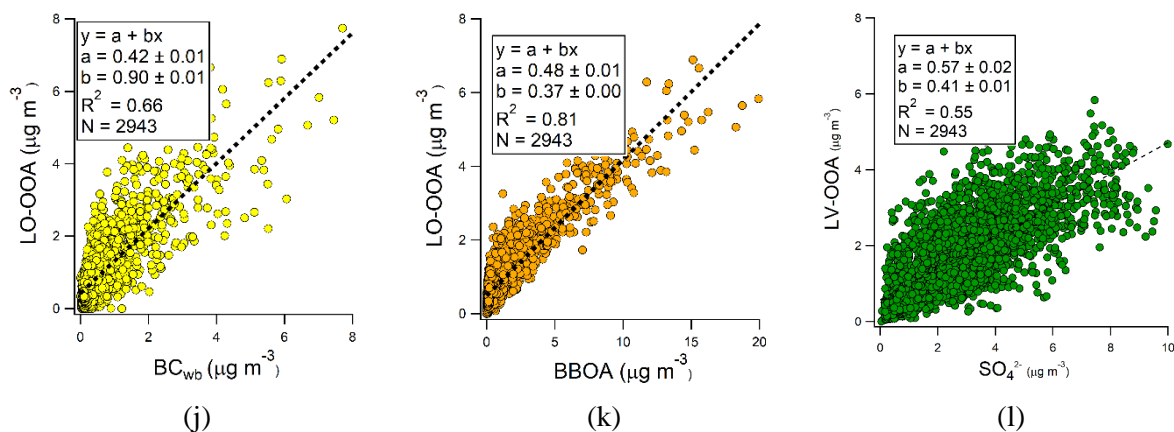
(g)



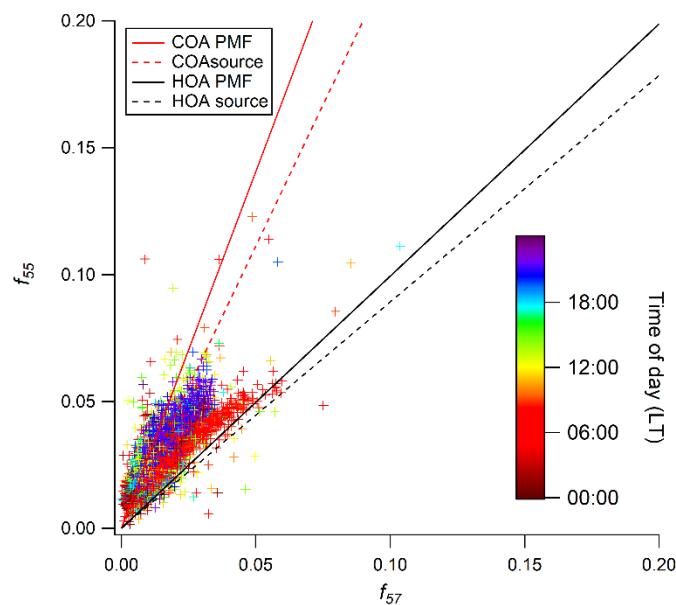
(h)



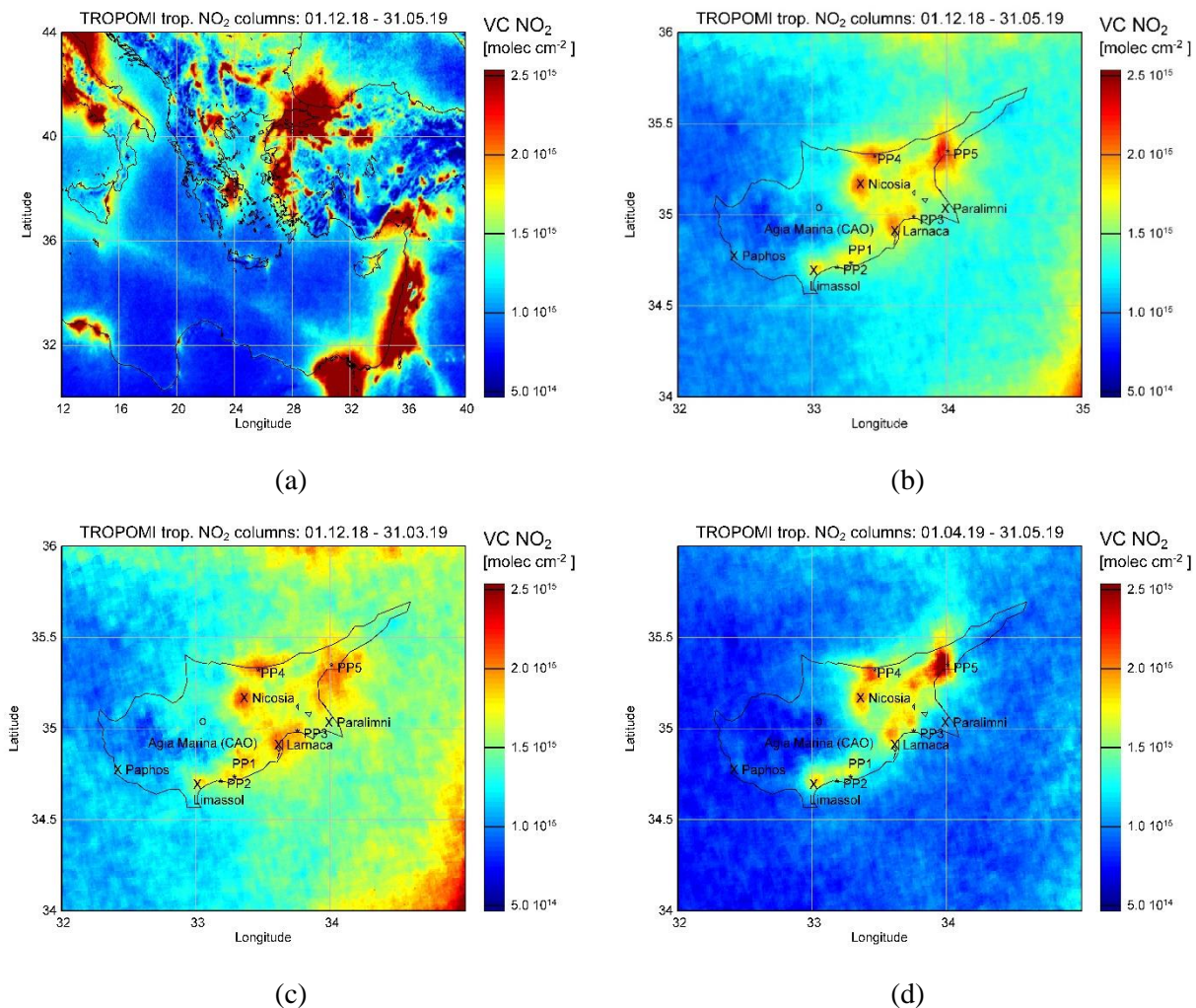
(i)



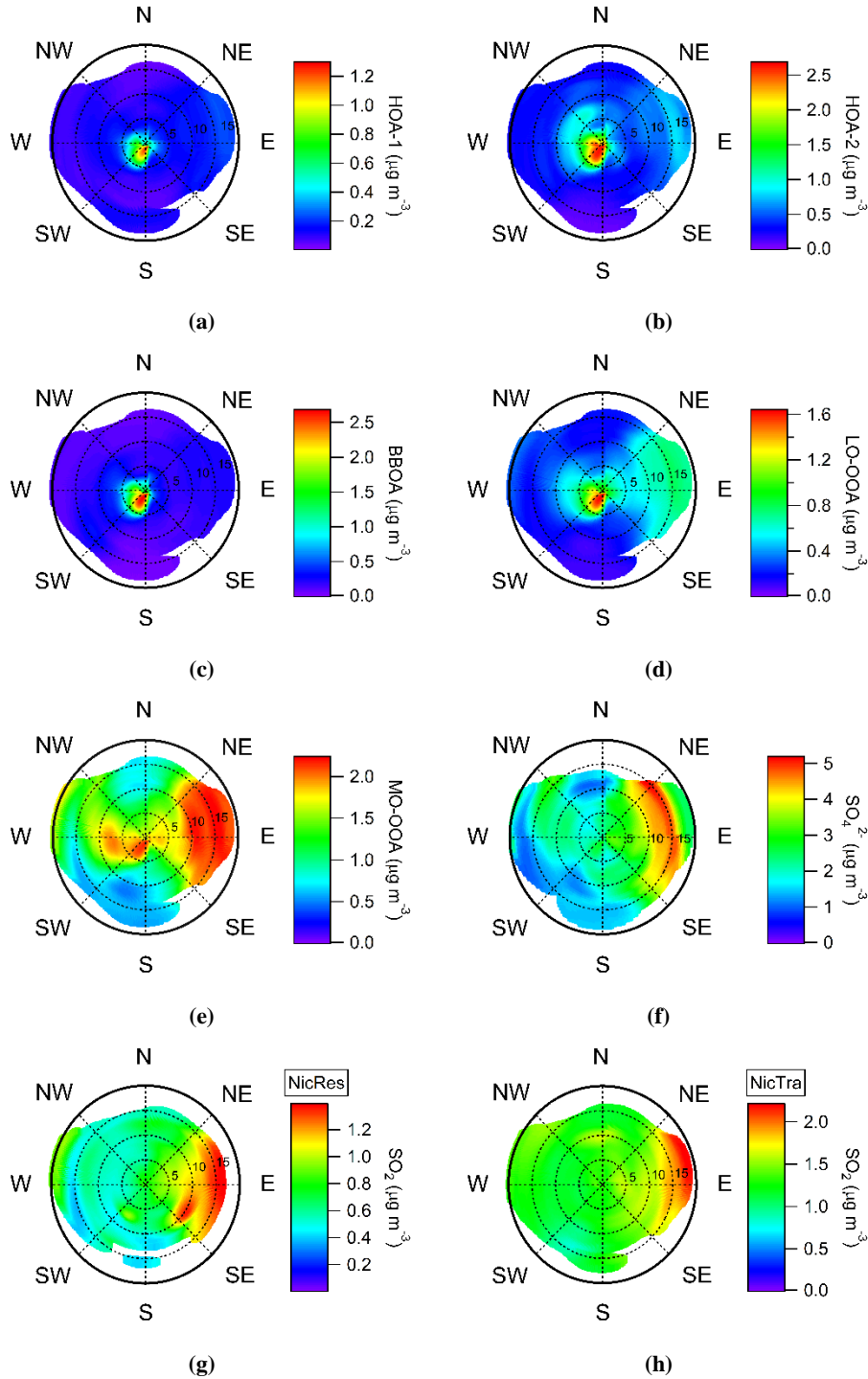
70 **Figure S11: Comparison of OA factor time series with external tracers during the cold period**



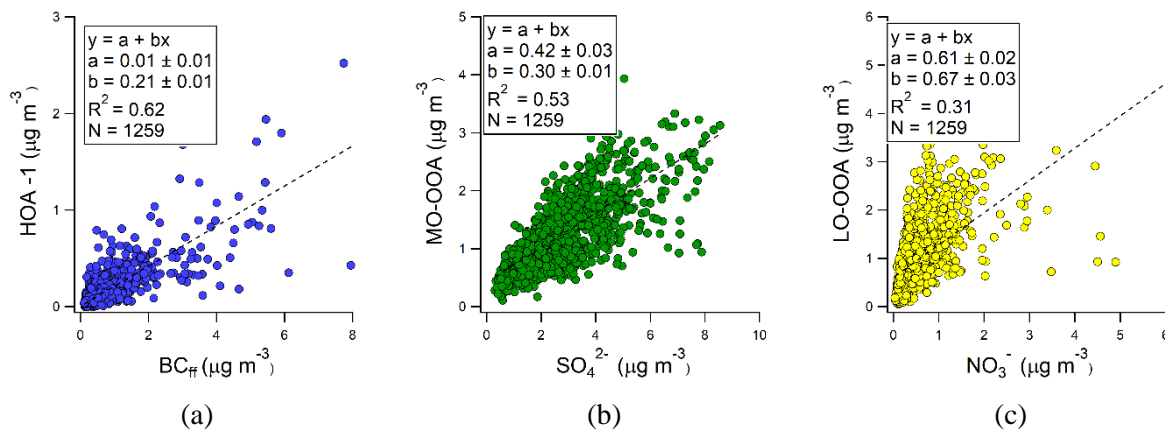
75 **Figure S12: Mass fraction of  $m/z$  55 and 57 ( $f_{55}$  and  $f_{57}$ ) for primary organics.  $f_{55}$  and  $f_{57}$  linear fits extracted from various PMF COA and HOA factors (red and black line accordingly), as well as from cooking and traffic source emission studies (red and black dashed line accordingly) reported in (Mohr et al., 2012). Data points are coloured according to time of day.**



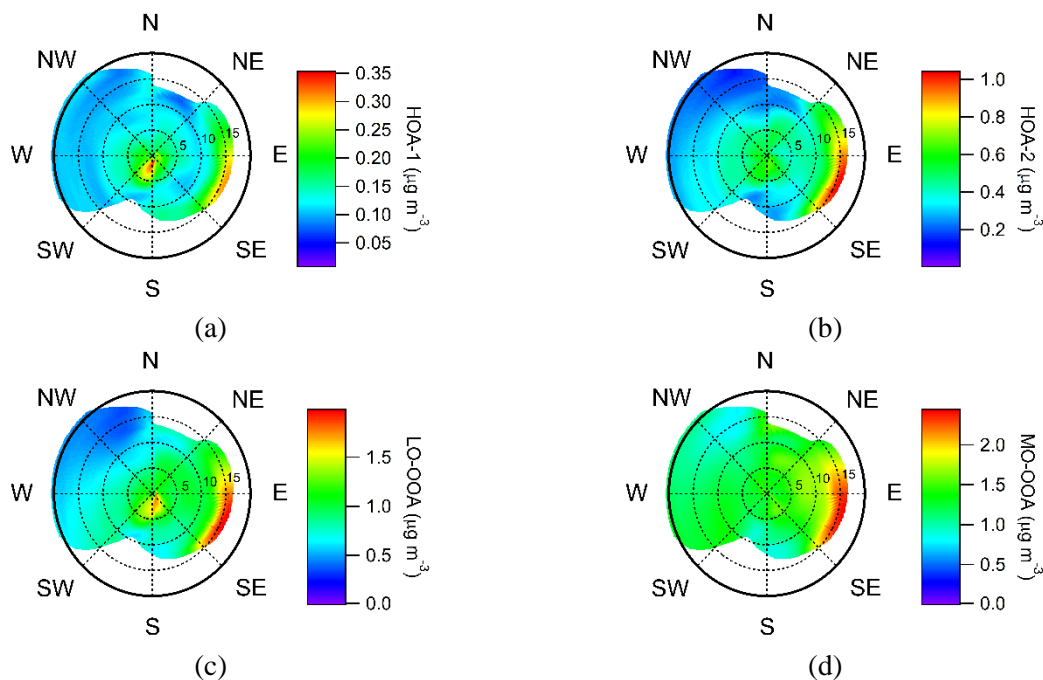
**Figure S13: Spatial variability of space-based (SP5-TROPOMI) vertical columns of NO<sub>2</sub> in the East Mediterranean (a) and Cyprus (b) for the entire period of the campaign. Cold and warm period (c and d) with the geolocation of the main urban centers and power plants in Cyprus and the location of the background station CAO (x Nicosia).**

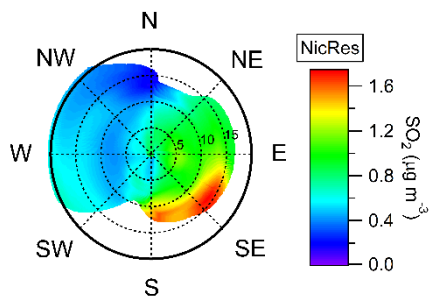


**Figure S14: Non-Parametric Wind (NWR) regression polar plots for (a) HOA-1, (b) HOA-2, (c) BBOA, (d) LO – OOA and (e) MO – OOA, calculated for the cold period in Nicosia. Non-Parametric Wind (NWR) regression polar plots calculated for f)  $\text{SO}_4^{2-}$  at the CAO-NIC (g)  $\text{SO}_2$  at the residential and (h)  $\text{SO}_2$  at the traffic site, for the cold period in Nicosia.**

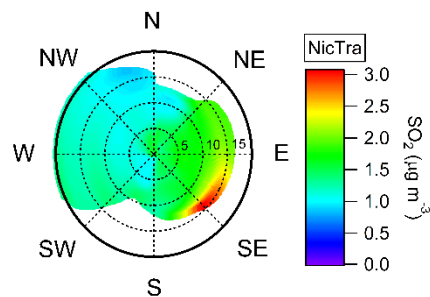


**Figure S15 Comparison of OA factor timeseries with external tracers during the warm period**





(e)



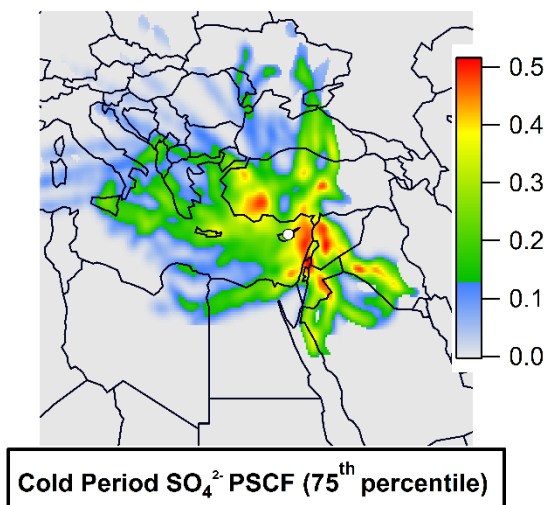
(f)

90 **Figure S16: Non-Parametric Wind (NWR) regression polar plots for (a) HOA-1, (b) HOA-2, (c) LO – OOA and (d) MO – OOA, calculated for the warm period in Nicosia. Non-Parametric Wind (NWR) regression polar plots calculated for (e) SO2 at the residential and (f) SO2 at the traffic site, for the warm period in Nicosia.**

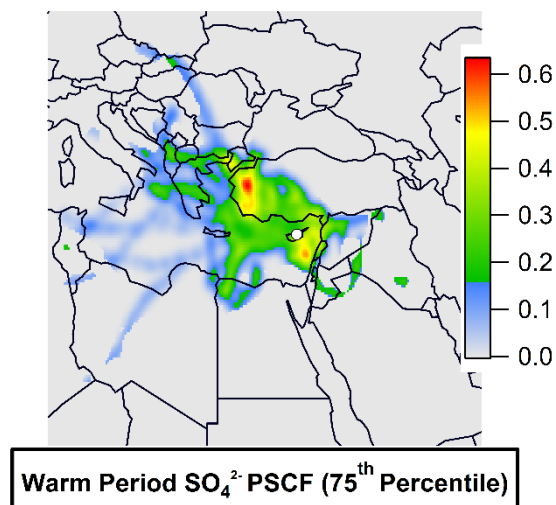
**Table S2: OA factor sources mean, standard deviation, median concentrations and respective contribution to total OA during cold and warm periods in Nicosia.**

	Cold Period				Warm Period			
$\mu\text{g m}^{-1}$	Mean	Std	Median	Contribution ( % )	Mean	Std	Median	Contribution ( % )
<b>HOA - 1</b>	0.46	0.93	0.17	7	0.17	1.91	0.11	6
<b>BBOA</b>	1.01	2.15	0.25	12	-	-	-	-
<b>HOA - 2</b>	1.33	2.07	0.61	21	0.45	0.56	0.34	16
<b>MO - OOA</b>	1.75	1.06	1.60	44	1.27	0.55	1.19	45
<b>LO - OOA</b>	0.86	0.88	0.58	16	0.95	0.11	0.60	34

95



(a)



(b)

**Figure S17: PSCF calculated for the 75<sup>th</sup> percentile for  $\text{SO}_4^{2-}$  for the (a) cold and (b) warm period respectively.**



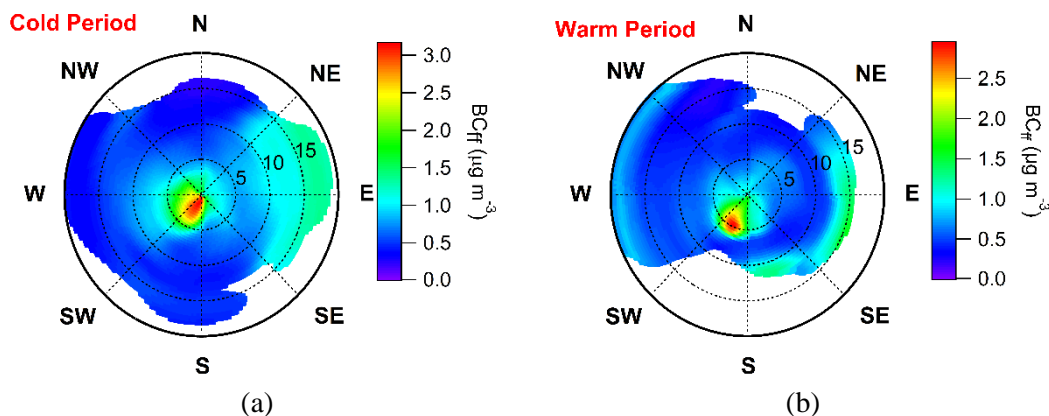


Figure S18. Non-Parametric Wind regression (NWR) polar plots calculated for  $BC_{ff}$  during the (a) cold and (b) warm period in Nicosia.

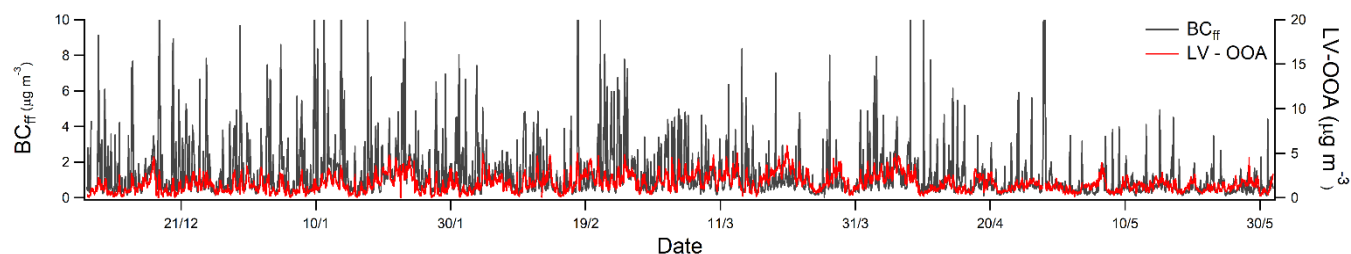


Figure S19: Temporal variability of  $BC_{ff}$  and MO-OOA concentrations during the entire measuring period.

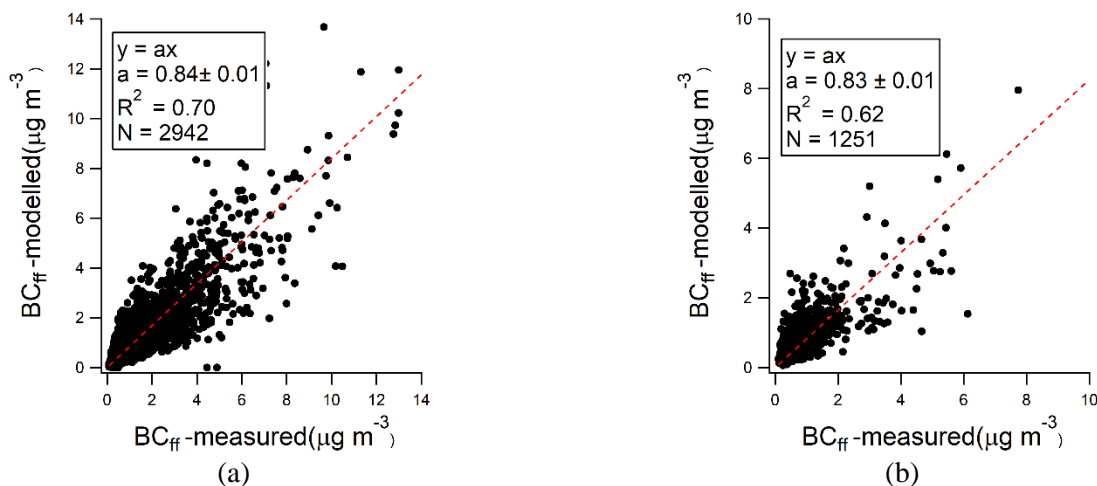
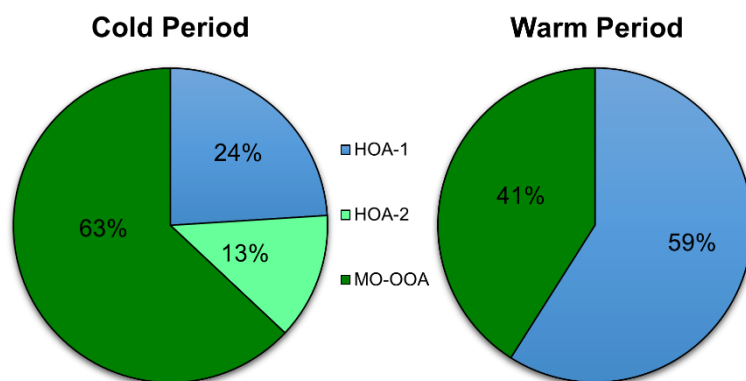


Figure S20: Correlation between measured and modelled  $BC_{ff}$  for the cold (a) and warm (b) period. The correlation curve (red lines) were calculated using the least orthogonal distance fit method.





**Figure S21:**  $BC_{II}$  contributions related to the sources retrieved from OA source apportionment for the cold (left) and warm (right) period.

## References

- Bougiatioti, A., Stavroulas, I., Kostenidou, E., Zarmpas, P., Theodosi, C., Kouvarakis, G., Canonaco, F., Prévôt, A. S. H., Nenes, A., Pandis, S. N., and Mihalopoulos, N.: Processing of biomass-burning aerosol in the eastern Mediterranean during summertime, *Atmos. Chem. Phys.*, <https://doi.org/10.5194/acp-14-4793-2014>, 2014.
- 115 Budisulistiorini, S. H., Canagaratna, M. R., Croteau, P. L., Marth, W. J., Baumann, K., Edgerton, E. S., Shaw, S. L., Knipping, E. M., Worsnop, D. R., Jayne, J. T., Gold, A., and Surratt, J. D.: Real-time continuous characterization of secondary organic aerosol derived from isoprene epoxydiols in downtown Atlanta, Georgia, using the aerodyne aerosol chemical speciation monitor, *Environ. Sci. Technol.*, 47, 5686–5694, <https://doi.org/10.1021/es400023n>, 2013.
- Crippa, M., Decarlo, P. F., Slowik, J. G., Mohr, C., Heringa, M. F., Chirico, R., Poulain, L., Freutel, F., Sciare, J., Cozic, J.,
- 120 Di Marco, C. F., Elsasser, M., Nicolas, J. B., Marchand, N., Abidi, E., Wiedensohler, A., Drewnick, F., Schneider, J., Borrmann, S., Nemitz, E., Zimmermann, R., Jaffrezo, J. L., Prévôt, A. S. H., and Baltensperger, U.: Wintertime aerosol chemical composition and source apportionment of the organic fraction in the metropolitan area of Paris, *Atmos. Chem. Phys.*, 13, 961–981, <https://doi.org/10.5194/acp-13-961-2013>, 2013.
- Crippa, M., Canonaco, F., Lanz, V. A., Äijälä, M., Allan, J. D., Carbone, S., Capes, G., Ceburnis, D., Dall'Osto, M., Day, D.
- 125 A., DeCarlo, P. F., Ehn, M., Eriksson, A., Freney, E., Ruiz, L. H., Hillamo, R., Jimenez, J. L., Junninen, H., Kiendler-Scharr, A., Kortelainen, A. M., Kulmala, M., Laaksonen, A., Mensah, A. A., Mohr, C., Nemitz, E., O'Dowd, C., Ovadnevaite, J., Pandis, S. N., Petäjä, T., Poulain, L., Saarikoski, S., Sellegri, K., Swietlicki, E., Tiitta, P., Worsnop, D. R., Baltensperger, U., and Prévôt, A. S. H.: Organic aerosol components derived from 25 AMS data sets across Europe using a consistent ME-2 based source apportionment approach, *Atmos. Chem. Phys.*, 14, 6159–6176, <https://doi.org/10.5194/acp-14-6159-2014>, 2014.
- 130 Florou, K., Papanastasiou, D. K., Pikridas, M., Kaltsonoudis, C., Louvaris, E., Gkatzelis, G. I., Patoulias, D., Mihalopoulos, N., and Pandis, S. N.: The contribution of wood burning and other pollution sources to wintertime organic aerosol levels in two Greek cities, *Atmos. Chem. Phys.*, 17, 3145–3163, <https://doi.org/10.5194/acp-17-3145-2017>, 2017.
- Gilardoni, S., Massoli, P., Paglione, M., Giulianelli, L., Carbone, C., Rinaldi, M., Decesari, S., Sandrini, S., Costabile, F., Gobbi, G. P., Pietrogrande, M. C., Visentin, M., Scotto, F., Fuzzi, S., and Facchini, M. C.: Direct observation of aqueous
- 135 secondary organic aerosol from biomass-burning emissions, *Proc. Natl. Acad. Sci. U. S. A.*, 113, 10013–10018, <https://doi.org/10.1073/pnas.1602212113>, 2016.
- Kaltsonoudis, C., Kostenidou, E., Louvaris, E., Psichoudaki, M., Tsiligiannis, E., Florou, K., Liangou, A., and Pandis, S. N.: Characterization of fresh and aged organic aerosol emissions from meat charbroiling, *Atmos. Chem. Phys.*, 17, 7143–7155, <https://doi.org/10.5194/acp-17-7143-2017>, 2017.
- 140 Kostenidou, E., Florou, K., Kaltsonoudis, C., Tsiflikiotou, M., Vratolis, S., Eleftheriadis, K., and Pandis, S. N.: Sources and chemical characterization of organic aerosol during the summer in the eastern Mediterranean, *Atmos. Chem. Phys.*, 15, 11355–11371, <https://doi.org/10.5194/acp-15-11355-2015>, 2015.
- Lanz, V. A., Prévôt, A. S. H., Alfarra, M. R., Weimer, S., Mohr, C., Decarlo, P. F., Gianini, M. F. D., Hueglin, C., Schneider,

- J., Favez, O., D'Anna, B., George, C., and Baltensperger, U.: Characterization of aerosol chemical composition with aerosol mass spectrometry in Central Europe: An overview, *Atmos. Chem. Phys.*, 10, 10453–10471, <https://doi.org/10.5194/acp-10-10453-2010>, 2010.
- Mohr, C., DeCarlo, P. F., Heringa, M. F., Chirico, R., Slowik, J. G., Richter, R., Reche, C., Alastuey, A., Querol, X., Seco, R., Peñuelas, J., Jiménez, J. L., Crippa, M., Zimmermann, R., Baltensperger, U., and Prévôt, A. S. H.: Identification and quantification of organic aerosol from cooking and other sources in Barcelona using aerosol mass spectrometer data, *Atmos. Chem. Phys.*, 12, 1649–1665, <https://doi.org/10.5194/acp-12-1649-2012>, 2012.
- Ng, N. L., Herndon, S. C., Trimborn, A. M., Canagaratna, M. R., Croteau, P. L., Onasch, T. B., Sueper, D., Worsnop, D. R., Zhang, Q., Sun, Y. L., and Jayne, J. T.: An Aerosol Chemical Speciation Monitor (ACSM) for routine monitoring of the composition and mass concentrations of ambient aerosol, *Aerosol Sci. Technol.*, 45, 780–794, <https://doi.org/10.1080/02786826.2011.560211>, 2011a.
- Ng, N. L., Canagaratna, M. R., Jimenez, J. L., Zhang, Q., Ulbrich, I. M., and Worsnop, D. R.: Real-time methods for estimating organic component mass concentrations from aerosol mass spectrometer data, *Environ. Sci. Technol.*, 45, 910–916, <https://doi.org/10.1021/es102951k>, 2011b.
- Paglionè, M., Gilardoni, S., Rinaldi, M., Decesari, S., Zanca, N., Sandrini, S., Giulianelli, L., Bacco, D., Ferrari, S., Poluzzi, V., Scotto, F., Trentini, A., Poulain, L., Herrmann, H., Wiedensohler, A., Canonaco, F., Prévôt, A. S. H., Massoli, P., Carbone, C., Facchini, M. C., and Fuzzi, S.: The impact of biomass burning and aqueous-phase processing on air quality: a multi-year source apportionment study in the Po Valley, Italy, *Atmos. Chem. Phys. Discuss.*, 1–37, <https://doi.org/10.5194/acp-2019-274>, 2019.
- Sage, A. M., Weitkamp, E. A., Robinson, A. L., and Donahue, N. M.: Evolving mass spectra of the oxidized component of organic aerosol: Results from aerosol mass spectrometer analyses of aged diesel emissions, *Atmos. Chem. Phys.*, 8, 1139–1152, <https://doi.org/10.5194/acp-8-1139-2008>, 2008.
- Stavroulas, I., Bougiatioti, A., Grivas, G., Paraskevopoulou, D., Tsagkaraki, M., Zarmpas, P., Liakakou, E., Gerasopoulos, E., and Mihalopoulos, N.: Sources and processes that control the submicron organic aerosol composition in an urban Mediterranean environment (Athens): A high temporal-resolution chemical composition measurement study, *Atmos. Chem. Phys.*, 19, 901–919, <https://doi.org/10.5194/acp-19-901-2019>, 2019.
- Stavroulas, I., Grivas, G., Liakakou, E., Kalkavouras, P., Bougiatioti, A., Kaskaoutis, D. G., Lianou, M., Papoutsidaki, K., Tsagkaraki, M., Zarmpas, P., Gerasopoulos, E., and Mihalopoulos, N.: Online chemical characterization and sources of submicron aerosol in the major mediterranean port city of piraeus, greece, *Atmosphere (Basel)*, 12, 1–28, <https://doi.org/10.3390/atmos12121686>, 2021.